Available online at www.sciencedirect.com
SCIENCE DIRECT®
Journal of Sound and Vibration 275 (2004) 1136–1146
JOURNAL OF SOUND AND VIBRATION
www.elsevier.com/locate/jsvi

Letter to the Editor

Chaos and bifurcations in a nonlinear vehicle model

Q. Zhu*, M. Ishitobi

Department of Mechanical Engineering and Materials Science, Faculty of Engineering, Kumamoto University, 2-39-1 Kurokami, Kumamoto 860-8555, Japan

Received 12 July 2002; accepted 20 October 2003

1. Introduction

Since the disturbance from the road may induce uncomfortable shake and noise in the vehicle body, it is important to study the vibrations of the vehicle. Many studies have been carried out on the dynamic response and the vibration control with linear mechanical model. However, an automobile is a non-linear system in practice because it consists of suspensions, tires and other components that have non-linear properties. Therefore, the chaotic response may appear as the vehicle moves over a bumpy road.

A vehicle can be modelled as a complex multi-body dynamic system. The degree of complexity depends on the aim of modelling. Several models have been developed in the researches related to the dynamic behavior of vehicle and its vibration control. The quarter-car model (2-d.o.f. system) for studying the heave motion [1–3], the half-car model (4-d.o.f. system) as a two-wheel (front and rear) model for studying the heave and pitch motions [4–6], and the full vehicle model (basically 7-d.o.f. system) as a four-wheel model for studying the heave, pitch and roll motions [7]. The 4-d.o.f. model allows the study of both the heave and pitch motions along with the deflection of tires and suspensions. All of these quantities are of great importance in the design of vehicle. Since the model is also relatively simple to analyze when compared to the 7-d.o.f. full 3-D vehicle model, and yet can reasonably predict the response of the latter [8], the 4-d.o.f. half-vehicle model is used by many researchers. In this paper, the chaotic vibration of the 4-d.o.f. half-vehicle model with non-linear spring and damping element is investigated. The study begins by introducing a non-linear 4-d.o.f. half-vehicle model. Next, the numerical simulation is conducted and the dynamic responses of the model are investigated. Resonance curves, bifurcation diagrams and Poincaré maps are used in the investigation. The dominant Lyapunov exponent is used to identify the chaotic motion of the system. The results indicate that the chaotic vibration may exist in the ground vehicle.

*Corresponding author. Fax: +81-96-342-3729.
E-mail address: zhu@mech.kumamoto-u.ac.jp (Q. Zhu).

0022-460X/$ - see front matter
doi:10.1016/j.jsv.2003.10.016

2. Simulation model

The longitudinal view of the 4-d.o.f. half-vehicle model with non-linear springs and dampers is illustrated in Fig. 1. The definition of symbols used is given in the appendix. The model consists of a rigid vehicle body, front and rear unsprung masses, springs and dampers of front and rear suspensions and tires. The vehicle body has rigid heave and pitch motions and the unsprung mass has only heave motions. The static equilibrium position is used as the origin for both heave displacement $x_b(t)$ and angular displacement of the vehicle body mass $\theta(t)$, and also for heave displacements of both front and rear unsprung mass, $x_f(t)$ and $x_r(t)$.

Suspension of the vehicle is simplified to non-linear spring and non-linear damper. The suspension spring is assumed to have the following characteristics:

$$f_s = k_s \,\mathrm{sgn}(\Delta_s)|\Delta_s|^n, \tag{1}$$

where f_s is the spring dynamic force, k_s is the equivalent stiffness, Δ_s is the deformation of the spring that can be calculated by the displacement of both extremes of the spring, and sgn(·) is the signum function. The unit of Δ_s is in cm and k_s in N/cm [4,9]. In Eq. (1), n is an exponent representing non-linearity of the spring and it is referred as the non-linear coefficient of the suspension spring. As an example, linear and non-linear relations between f_s and Δ_s are shown in Fig. 2 where f_s is plotted with solid line as $n = 1.4$. The dashed line in this figure is the characteristics of a linear spring as $n = 1$.

The non-linear damping forces of suspensions is given by

$$f_{sc} = c_s \Delta \dot{x}_s, \tag{2}$$

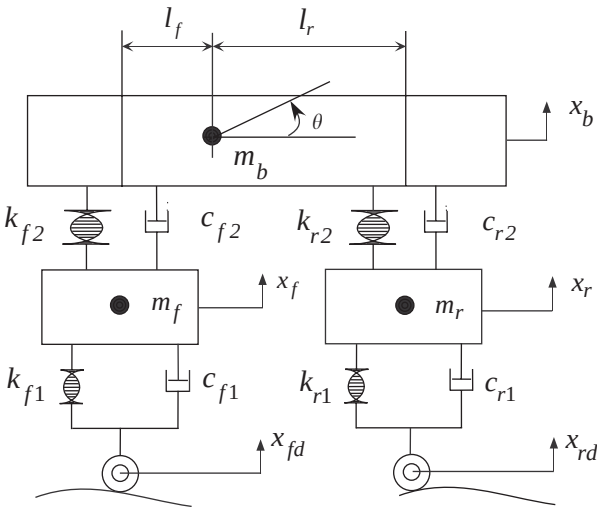

Fig. 1. Non-linear half-vehicle model.

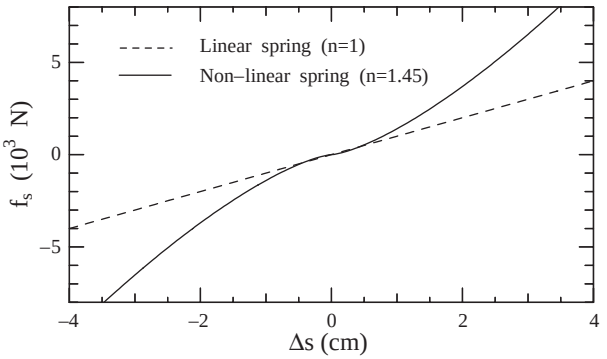

Fig. 2. Non-linear characteristics of the suspension and tire spring.

where f_{sc} is the damping force and $\Delta\dot{x}_s$ is the relative velocity of the extremes of the damper. The damping coefficient c_s is expressed by

$$c_s = \begin{cases} c_u, & \Delta\dot{x}_s \geqslant 0, \\ c_d, & \Delta\dot{x}_s < 0, \end{cases} \tag{3}$$

where c_u and c_d are damping coefficients for tension and compression, respectively.

The tire of the vehicle is also modelled by a non-linear spring. The spring force of the tire is expressed by Eq. (1) but with a smaller value of the exponent n. The damping of the tires is assumed to be viscous damping, then the damping force is calculated as

$$f_{tc} = c_t \Delta\dot{x}_t, \tag{4}$$

where c_t is the viscous damping coefficient and $\Delta\dot{x}_t$ is the relative velocity of extremes of the damper.

The sinusoid forcing function is used to describe the excitations caused by road surface. Thus, the road roughness is approximated by the equation

$$x_{fd} = A\sin(2\pi ft), \tag{5}$$

where A and f is the amplitude and the frequency of the sinusoid road disturbance, respectively. The excitation to the rear tire is defined as

$$x_{rd} = A\sin(2\pi ft + \alpha), \tag{6}$$

where α is related to the time delay between the forcing functions x_{fd} and x_{rd}.

By applying Newton's second law, the equation of the heave motion of the vehicle body can be expressed as

$$\begin{aligned} m_b\ddot{x}_b = & -k_{f2}\,\mathrm{sgn}(D_{bf2})|D_{bf2}|^{n_{f2}} - c_{f2}(\dot{x}_b - \dot{x}_f - l_f\dot{\theta}\cos\theta) \\ & - k_{r2}\,\mathrm{sgn}(D_{br2})|D_{br2}|^{n_{r2}} - c_{r2}(\dot{x}_b - \dot{x}_r + l_r\dot{\theta}\cos\theta) - m_b g \end{aligned} \tag{7}$$

and the equation of motion for pitch is

$$J\ddot{\theta} = [k_{f2}\,\mathrm{sgn}(D_{bf2})|D_{bf2}|^{n_{f2}} + c_{f2}(\dot{x}_b - \dot{x}_f - l_f\dot{\theta}\cos\theta)]l_f\cos\theta - [k_{r2}\,\mathrm{sgn}(D_{br2})|D_{br2}|^{n_{r2}} + c_{r2}(\dot{x}_b - \dot{x}_r + l_r\dot{\theta}\cos\theta)]l_r\cos\theta, \quad (8)$$

where

$$D_{bf2} = x_b - \Delta_{sf2} - x_f - l_f\sin\theta,$$
$$D_{br2} = x_b - \Delta_{sr2} - x_r + l_r\sin\theta.$$

In above expressions, Δ_{sf2} and Δ_{sr2} denote static deformation of the suspension spring with stiffness k_{f2} and k_{r2}. The damping coefficients c_{f2} and c_{r2} are defined by Eq. (3).

By applying Newton's second law again on the front and rear unsprung masses, the equations of motion can be formulated.

Front wheel:

$$m_f\ddot{x}_f = k_{f2}\,\mathrm{sgn}(D_{bf2})|D_{bf2}|^{n_{f2}} + c_{f2}(\dot{x}_b - \dot{x}_f - l_f\dot{\theta}\cos\theta) - k_{f1}\,\mathrm{sgn}(x_f - \Delta_{sf1} - x_{fd})|x_f - \Delta_{sf1} - x_{fd}|^{n_{f1}} - c_{f1}(\dot{x}_f - \dot{x}_{fd}) - m_f g. \quad (9)$$

Rear wheel:

$$m_r\ddot{x}_r = k_{r2}\,\mathrm{sgn}(D_{br2})|D_{br2}|^{n_{r2}} + c_{r2}(\dot{x}_b - \dot{x}_r + l_r\dot{\theta}\cos\theta) - k_{r1}\,\mathrm{sgn}(x_r - \Delta_{sr1} - x_{rd})|x_r - \Delta_{sr1} - x_{rd}|^{n_{r1}} - c_{r1}(\dot{x}_r - \dot{x}_{rd}) - m_r g, \quad (10)$$

where Δ_{sf1} and Δ_{sr1} are static deformation of the tire spring with stiffness k_{f1} and k_{r1}. The static deformations Δ_{sfi} and Δ_{sri} $(i = 1, 2)$ can be evaluated by Eq. (1).

3. Numerical results

Owing to the non-linearity of the differential equations (7)–(10), the dynamic response of the vehicle model was studied numerically with the fourth order Runge–Kutta algorithm provided by MATLAB. In the computation, the absolute error tolerance was less than 10^{-6}. Since numerical integration could give spurious results with regard to the existence of chaos due to insufficiently small time steps [10], the step size was verified to ensure no such results were generated as a result of time discretization. The vehicle parameter set assumed for the numerical study is shown in Table 1.

It is known that the dynamics of a system may be analyzed through a frequency-response diagram, which is obtained by plotting the amplitude of the oscillating system versus the frequency of the excitation term [11,12]. For the studied system, the frequency-response diagram was calculated numerically. The amplitude was defined as the maximum absolute value of the displacement and the control parameter was defined as the forcing frequency of the excitation from road surface.

Fig. 3 represents one of the frequency-response diagrams of the model when the forcing frequency f is slowly increased and decreased. The damping coefficients were $c_{f2u} = c_{r2u} = 500$ kg/s,

Table 1
Parameters for numerical simulation

m_b	1180.0 kg
J	633.615 kg m^2
m_f	50.0 kg
m_r	45.0 kg
l_f	1.123 m
l_r	1.377 m
k_{f2}	36 952.0 N/m
k_{r2}	30 130.0 N/m
k_{f1}	140 000.0 N/m
k_{r1}	140 000.0 N/m
n_{f2}	1.5
n_{r2}	1.5
n_{f1}	1.25
n_{r1}	1.25

$c_{f2u}/c_{f2d} = c_{r2u}/c_{r2d} = 1.39$, $c_{f1} = c_{r1} = 10$ kg/s and amplitude of the forcing function $A = 0.08$ m, respectively. The diagrams were calculated by using an increment $\Delta f = 0.01$ Hz as the variation of the control parameter. As illustrated in Figs. 3(a), (c) and (d), the frequency-response diagrams of the heave motion of vehicle body and the two unsprung masses are similar. The first jump is observed at $f = 3.6$ Hz, then the second jump is at $f = 4.6$ Hz as forcing frequency increased. The phenomenon of the two jumps can also be observed in response diagram of the pitch motion of vehicle body shown in Fig. 3(b). However, this diagram exhibits a more complicated and different behavior. This is confirmed by the presence of more jumps in the diagram as the forcing frequency increased or decreased. Fig. 3 shows that the responses of the system have instability region as $3.0 < f < 5.4$ Hz, which indicates that the chaotic responses are possible when the forcing frequency is within or near the instable region [13–15].

A widely used technique for examining the changes of responses in a dynamic system under parameter variations is the bifurcation diagram. To make the bifurcation diagram, some measure of the motion is plotted as a function of a system parameter [16]. In this study, the bifurcation diagram is obtained by plotting the Poncaré points of the displacement and one of the system parameters.

As shown in Fig. 4, the bifurcation diagram is obtained by plotting the Poncaré points of the displacement $\theta(t)$ against the damping coefficient c_{r2u}. The parameters of excitation and damping coefficients used in the computation were $A = 0.08$ m, $f = 3.6$ Hz, $\alpha = \pi/9$ rad, $c_{f2u} = 500$ kg/s, $c_{f2u}/c_{f2d} = 1.39$, $c_{r2d} = 360$ kg/s and $c_{f1} = c_{r1} = 10$ kg/s. In this diagram, c_{r2u} varied from 0 to 3000 kg/s according to 150 equal steps. For every parameter c_{r2u}, the responses of the system from 0 to 400 s that was 1440 forcing cycles, were computed. To eliminate the transient responses, only the last 250 points of the Poincaré section associated with the 250 last periods were saved. The initial conditions were set to zeros for every parameter. The different behavior was observed as the values of c_{r2u} were in the range of 0–3000 kg/s. In Fig. 4, we observed that the responses of the system could become chaotic very quickly as the coefficient c_{r2u} is around 200 kg/s. This implies that the periodic responses of the model may jump to chaotic one even there is only a small change in damping coefficients.

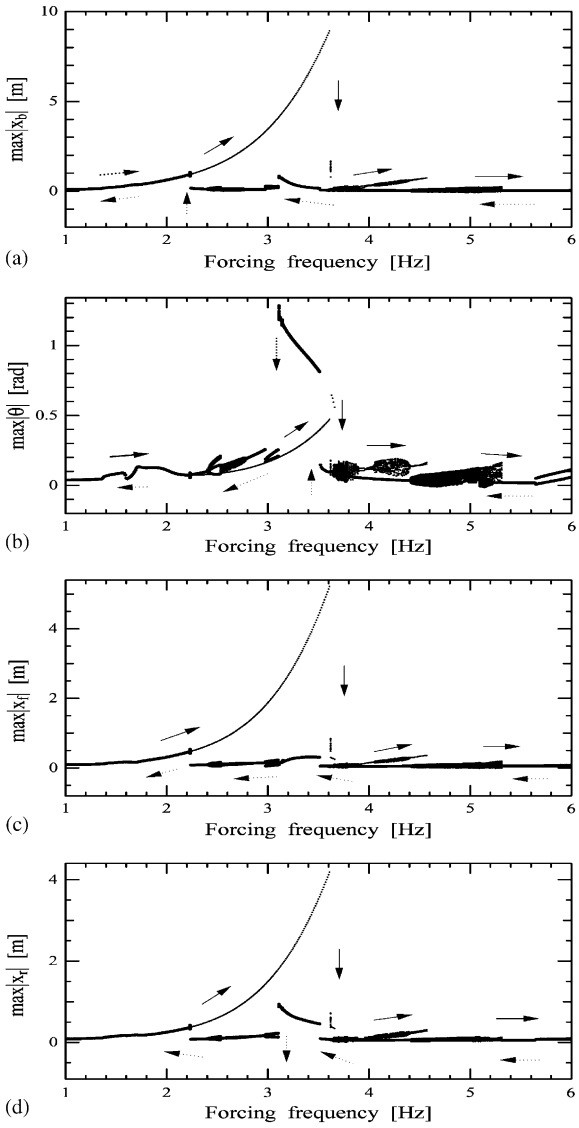

Fig. 3. Frequency-response diagrams when the forcing frequency f is slowly increased and decreased ($A = 0.08$ m, $\alpha = \pi/9$, $0 < f < 6$ Hz, the remaining parameters are shown in Table 1): (a) $\max|x_b(t)|$; (b) $\max|\theta(t)|$; (c) $\max|x_f(t)|$, and (d) $\max|x_r(t)|$.

Fig. 5 represents the bifurcation of $\theta(t)$ by varying the values of the parameter α from 0° to 360°. The increment of α was 1°. The time span for the computation was from 0 to 400 s. The initial condition was set to zero. As the computation for Fig. 4, the last 250 Poincaré points were preserved for plotting the diagram. The enlargements of the bifurcation diagram in Fig. 5 are shown in Figs. 6(a) and (b). These bifurcation diagrams exhibit period windows and crisis as the time delay α is around $0 < \alpha < \pi/3$ and $1.6\pi < \alpha < 2\pi$.

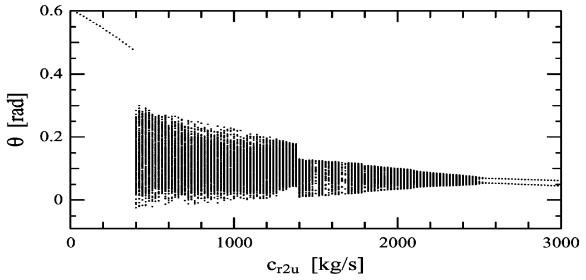

Fig. 4. Bifurcation diagram of $\theta(t)$ as a function of c_{r2u} ($0 \leqslant c_{r2u} \leqslant 3000$ kg/s).

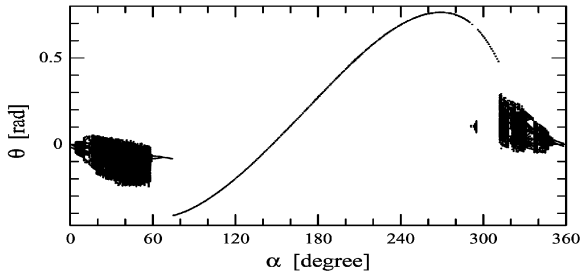

Fig. 5. Bifurcation diagram of $\theta(t)$ obtained by varying α ($0 \leqslant \alpha \leqslant 2\pi$).

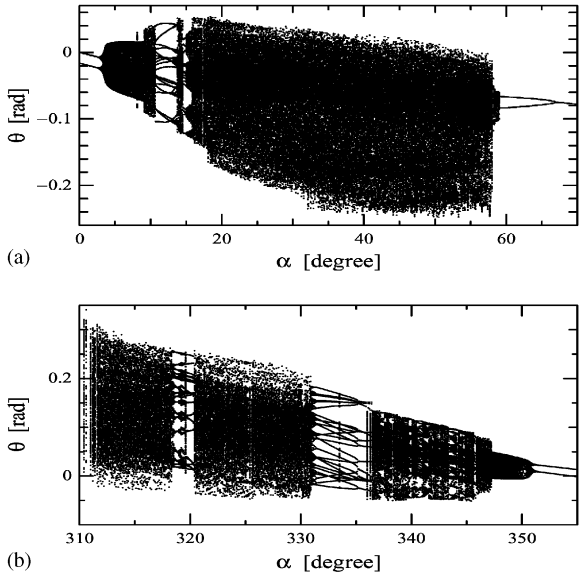

Fig. 6. Enlargements of the bifurcation diagram of Fig. 5.

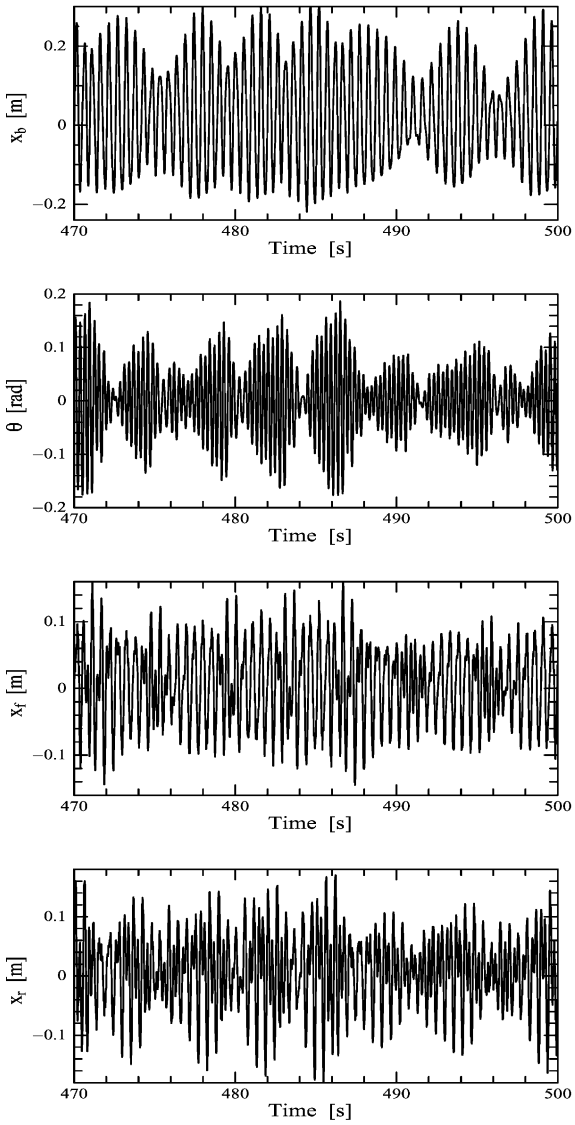

Fig. 7. Time histories of chaotic motion of the system ($A = 0.08$ m, $f = 3.6$ Hz, $\alpha = \pi/9$ rad, the remaining parameters are shown in Table 1).

One of the time histories of $x_b(t)$, $\theta(t)$, $x_f(t)$ and $x_r(t)$ are plotted in Fig. 7. The time history data of the first 1600 forcing cycles were not used in order to guarantee that the data used were in a steady state. To determine whether the responses in these figures were chaotic, the method by investigating correlation dimension D_2 and the dominant Lyapunov exponent was implemented [17]. The Grassberger–Procaccia algorithm [18,19] was used to estimate D_2 and Wolf's algorithm [20] was used to calculate the dominant Lyapunov exponent. The time histories of $x_b(t)$, $\theta(t)$, $x_f(t)$ and $x_r(t)$ were sampled with a sampling period of 0.0043 s and each datum was 10^5 samples long.

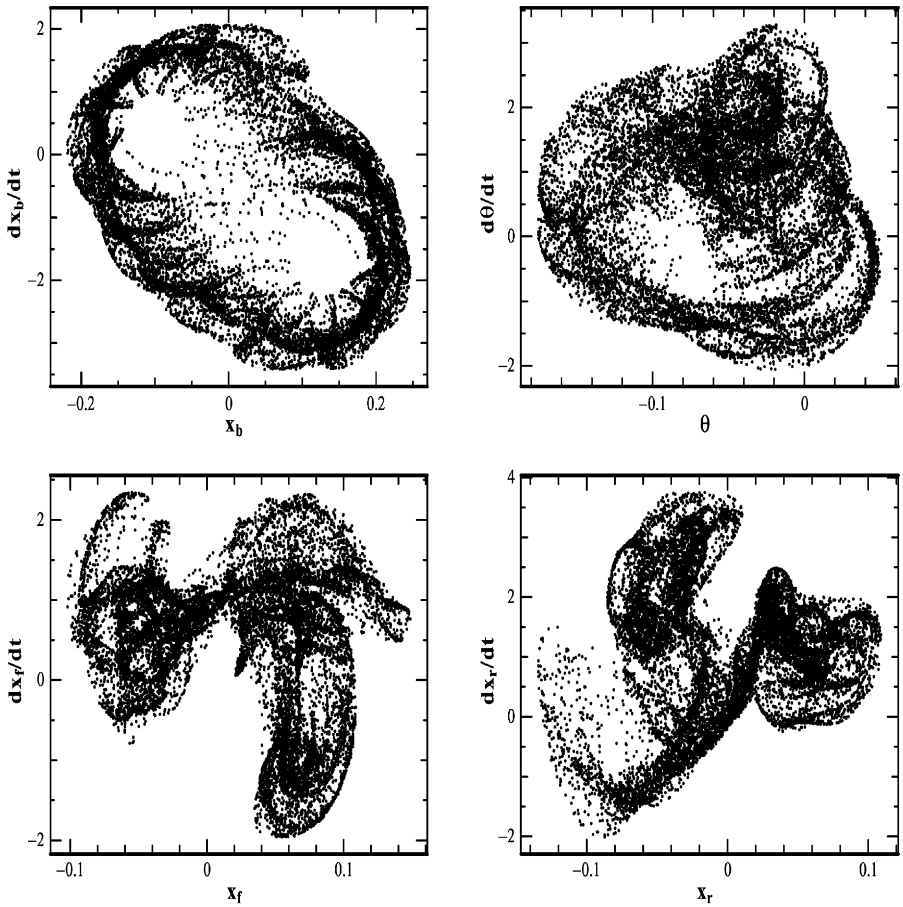

Fig. 8. Poincaré maps of chaotic motion of the system ($A = 0.08$ m, $f = 3.6$ Hz, $\alpha = \pi/9$ rad).

To create time-embedded vectors in the computation, the value of time delay was determined by the use of average mutual information [21]. The computation gave the values of D_2 for $D_{2x_b} = 2.02$, $D_{2\theta} = 1.64$, $D_{2x_f} = 2.01$, and $D_{2x_r} = 1.69$, respectively. On the other hand, the dominant Lyapunov exponents calculated were $\lambda_{x_b} = 0.78$, $\lambda_\theta = 6.32$, $\lambda_{x_f} = 2.32$, and $\lambda_{x_r} = 3.93$ in the unit of bits/s. The Poincaré maps of the responses of the system corresponding to time histories in Fig. 7 are shown in Fig. 8. Each Poincaré map contains 4300 sampling points. Fig. 8 shows that the strange attractors exist. These results indicated that the responses of the system were chaotic.

4. Conclusions

The chaotic responses and bifurcations of a four-degree-of-freedom vehicle model that is subjected to two sinusoid disturbance with time delay are studied through numerical simulation. It is found that the chaotic response may appear in the instable region of frequency-response

diagram. The bifurcation diagram shows that the chaotic response could be sensitive to variation of damping of the suspension. Although the mechanical model of the vehicle is only a simplified one and the parameters used do not agree closely with the practical data for an automobile, the results may still be useful in dynamic design of the ground vehicle. The confirmation of the existence of the chaos in this kind of model by experiment is left for further study.

Appendix. Nomenclature

m_b	vehicle body mass
J	vehicle body inertia
m_f	front unsprung mass
m_r	rear unsprung mass
$x_b(t)$	displacement of m_b
$\theta(t)$	angular displacement of m_b
$x_f(t)$	displacement of m_f
$x_r(t)$	displacement of m_r
$x_{fd}(t)$	excitation to the front tire
$x_{rd}(t)$	excitation to the rear tire
l_f	front length
l_r	rear length
k_{f2}	front suspension spring stiffness
c_{f2}	front suspension damping
k_{r2}	rear suspension spring stiffness
c_{r2}	rear suspension damping
k_{f1}	front tire stiffness
c_{f1}	front tire damping
k_{r1}	rear tire stiffness
c_{r1}	rear tire damping

References

[1] J.D. Robson, Road surface description and vehicle response, *International Journal of Vehicle Design* 9 (1979) 25–35.

[2] J. Yang, Y. Suematsu, Z. Kang, Two-degree-of-freedom controller to reduce the vibration of vehicle engine-body system, *IEEE Transactions on Control Systems Technology* 9 (2001) 295–317.

[3] R.A. Williams, Automotive active suspensions, Part 1: basic principles, *Proceedings of the Institute of Mechanical Engineers, Journal of Automobile Engineering, Proceedings Part D* 211 (1997) 415–426.

[4] A. Moran, M. Nagai, Optimal active control of nonlinear vehicle suspension using neural networks, *JSME International Journal, Series C* 37 (1994) 707–718.

[5] D. Vetturi, M. Gadola, D. Cambiaghi, L. Manzo, Semi-active strategies for racing car suspension control, *II Motorsports Engineering Conference and Exposition*, Dearborn (USA), SAE Technical Papers, No. 962553, December 1996.

[6] J. Campos, L. Davis, F.L. Lewis, S. Ikenaga, S. Scully, M. Evans, Active suspension control of ground vehicle heave and pitch motions, in: *Proceedings of the Seventh IEEE Mediterranean Control Conference on Control and Automation*, Haifa, Israel, June 1999, pp. 222–233.
[7] S. Ikenaga, F.L. Lewis, J. Campos, L. Davis, Active suspension control of ground vehicle based on a full-vehicle model, *Proceedings of America Control Conference*, Chicago, IL, USA, June 2000.
[8] F. Oueslati, S. Sankar, A class of semi-active suspension schemes for vehicle vibration control, *Journal of Sound and Vibration* 173 (3) (1994) 391–411.
[9] J.C. Dixon, *Tires, Suspension and Handling*, 2nd Edition, Society of Automotive Engineers, Warrendale, PA, 1996.
[10] B.H. Tongue, Characteristics of numerical simulations of chaotic system, *American Society of Mechanical Engineers Journal of Applied Mechanics* 54 (1987) 695–699.
[11] J.M.T. Thompson, H.B. Stewart, *Nonlinear Dynamics and Chaos*, Wiley, New York, 1986.
[12] D. Belato, H.I. Weber, J.M. Balthazar, M.D.T. Mook, Chaotic vibration of a nonideal electro-mechanical system, *International Journal of Solids and Structures* 38 (2001) 1699–1706.
[13] Q. Zhu, J. Tani, T. Takagi, Chaotic vibrations of a magnetically levitated system with two degrees of freedom, *Journal of Technical Physics* 35 (1994) 171–184.
[14] G. Haller, *Chaos Near Resonance*, Springer, Berlin, 1999.
[15] L. Pùst, O. Szöllös, The forced chaotic and irregular oscillations of the nonlinear two degrees of freedom (2dof) system, *International Journal of Bifurcation and Chaos* 9 (1999) 479–491.
[16] F.C. Moon, *Chaotic and Fractal Dynamics*, Wiley, New York, 1992.
[17] S. Haykin, S. Puthusserypady, Chaotic dynamics of sea clutter, *Chaos* 7 (1997) 777–802.
[18] P. Grassberger, I. Procaccia, Characterization of strange attractors, *Physical Review Letters* 50 (1983) 346–349.
[19] H. Takayasu (Ed.), *Fractal Science*, Asakura Shoten, Tokyo, 1987 (in Japanese).
[20] A. Wolf, J.B. Swift, H.L. Swinney, J.A. Vastano, Determining Lyapunov exponents from a time series, *Physica D* 16 (1985) 285–317.
[21] A.M. Fraser, H.L. Swinney, Independent coordinates for strange attractors from mutual information, *Physical Review A* 33 (1986) 1134–1140.